Time Series Land Cover Mapping and Change Detection Analysis Using Geographic Information System and Remote Sensing, Northern Ethiopia

Authors: Ayele, Gebiaw T, Tebeje, Aschalew K, Demissie, Solomon S, Belete, Mulugeta A, Jemberrie, Mengistu A, et al.

Source: Air, Soil and Water Research, 11(1)

Published By: SAGE Publishing

URL: https://doi.org/10.1177/1178622117751603

Time Series Land Cover Mapping and Change Detection Analysis Using Geographic Information System and Remote Sensing, Northern Ethiopia

Air, Soil and Water Research
Volume 11: 1–18

DOI: 10.1177/1178622117751603
SAGE

Gebiaw T Ayele[1], Aschalew K Tebeje[2], Solomon S Demissie[3], Mulugeta A Belete[4], Mengistu A Jemberrie[5], Wondie M Teshome[6], Dereje T Mengistu[7] and Engidasew Z Teshale[8]

[1]Australian Rivers Institute and School of Engineering, Griffith University, Nathan, QLD, Australia. [2]Amhara Design and Supervision Works Enterprise, Bahir Dar, Ethiopia. [3]Department of Civil and Environmental Engineering, UCLA, Los Angeles, CA, USA. [4]Faculty of Civil and Water Resources Engineering, Bahir Dar University, Bahir Dar, Ethiopia. [5]School of Civil Engineering and Architecture, Adama Science and Technology University, Adama, Ethiopia. [6]Faculty of Natural and Computational Sciences, Debre Tabor University, Debre Tabor, Ethiopia. [7]Amhara Water Works Construction Enterprise, Bahir Dar, Ethiopia. [8]Ethiopian Ministry of Water Resources, Addis Ababa, Ethiopia.

ABSTRACT: Land use planners require up-to-date and spatially accurate time series land resources information and changing pattern for future management. As a result, assessing the status of land cover change due to population growth and arable expansion, land degradation and poor resource management, partial implementation of policy strategies, and poorly planned infrastructural development is essential. Thus, the objective of the study was to quantify the spatiotemporal dynamics of land use land cover change between 1995 and 2014 using 5 multi-temporal cloud-free Landsat Thematic Mapper images. The maximum likelihood (ML)-supervised classification technique was applied to create signature classes for significant land cover categories using means and variances of the training data to estimate the probability that a pixel is a member of a class. The final Bayesian ML classification resulted in 12 major land cover units, and the spatiotemporal change was quantified using post-classification and statistical change detection techniques. For a period of 20 years, there was a continuously increasing demand for arable areas, which can be represented by an exponential growth model. Excepting the year 2009, the built-up area has shown a steady increase due to population growth and its need for infrastructure development. There was nearly a constant trend for water bodies with a change in slope significantly less than +0.01%. The 2014 land cover change statistics revealed that the area was mainly covered by cultivated, wood, bush, shrub, grass, and forest land mapping units accounting nearly 63%, 12%, 8%, 6%, 4%, and 2% of the total, respectively. Land cover change with agro-climatic zones, soil types, and slope classes was common in most part of the area and the conversion of grazing land into plantation trees and closure area development were major changes in the past 20 years.

KEYWORDS: remote sensing, land cover change detection, Landsat TM, ML, NDVI, PCC

RECEIVED: July 31, 2017. **ACCEPTED:** December 2, 2017.

TYPE: Original Research

FUNDING: The author(s) disclosed receipt of the following financial support for the research, authorship, and/or publication of this article: financial support for this research is received from Bahir Dar University–Blue Nile Water Institute: Grant number: 1/26971/1.11.10.

DECLARATION OF CONFLICTING INTERESTS: The author(s) declared no potential conflicts of interest with respect to the research, authorship, and/or publication of this article.

CORRESPONDING AUTHOR: Gebiaw T Ayele, Australian Rivers Institute and School of Engineering, Griffith University, Nathan, QLD 4111, Australia.
Email: g.ayele@griffith.edu.au; gebeyaw21@gmail.com

Introduction

Numerous studies have shown that there remain only few landscapes, peripheral and fairly inaccessible location, on the earth that are still in their natural state.[1] These changes are attributed to the human-caused environmental challenge that creates regional combinations of environmental conditions that may fall outside the envelope in the near future.[2] One of the most significant global challenges is related to management of the transformation of the earth's surface that occurs due to changes in land use.[3] As a result, land use land cover (LULC) change studies become an essential part of environmental and natural resource management.[4]

Ethiopia is part of the dynamic land cover change where more than 90% of the country's highlands were once forested, and currently the percentage of forest cover is less than 4%.[5] The land cover change in the study area and the country at large was an outcome of natural and socioeconomic factors and their utilization by man both in time and space.[6] Most importantly, population growth and agricultural and urban expansion are the major drivers of land cover change in the country.[7]

Understanding the spatiotemporal land cover status of an area is an important procedure to implement future conservation measures. This requires an in-depth analysis of time series fine-scale satellite images[8,9] as a vital tool to trace the trend and nature of land cover change.[10] As a result, 5 multi-temporal Landsat Thematic Mapper (TM) images were used to distinguish the different land cover types and classify large geographic areas employing change detection analysis.[11–13] The main objective of the change detection process based on digital images is to mathematicize the LULC change for different features of interest for varying time resolutions.[14] The techniques for change detection analysis included post-classification comparison (PCC), image ratio, and manual on-screen digitization of change, principal components analysis, image

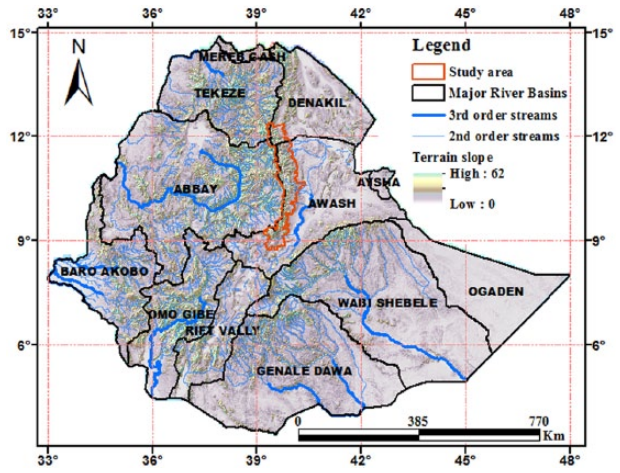

Figure 1. Location map of the study area: terrain slope, geographical setting of major river basins, and third-order and second-order network of streams.

regression, conventional image differentiation, and multi-date image classification.[15]

Supervised classifications require a priori knowledge of the scene area and regions containing a material of interest, training sites, and are delineated and stored for use in the supervised classification algorithm. The maximum likelihood (ML)-supervised classification techniques works with the assumption of assignment of each pixel to the LULC class for which they have the highest membership probability. The accuracy of pixel probabilistic classification can be further softened using posterior membership probability values.[16] Pixel probabilities are equal for all classes, and the input data in each band follow the Gaussian normal distribution function.[17] Although the ML method uses well-developed probability theory, the classification basic assumption has some drawbacks if the histogram of the image fails to follow the normal distribution curve. In addition, insufficient ground truth data would lead to erroneous estimation of the mean vector and the variance-covariance matrix, which results in poor image classification.[18] One of the particular problem in digital image processing and accurate land cover classification is the mountain topography shadowing effect which was improved using ancillary data, such as a digital elevation model and geomorphometric variables (relief, convexity, slope, aspects, and incidence).[7]

Land cover alterations are caused by poor management of land resources which lead to severe environmental problems. To understand situations of unrecorded land use change, interpretation of data from earth-sensing satellites has become vital. The LULC changes can be monitored at different spatiotemporal scales using geographic information system (GIS) and remote sensing (RS)[19,20] tools that provide scientific procedures to analyse the pattern, rate, and trend of environmental change at all scales.[21] Satellite images are the most common data source for change detection, quantification, and mapping of land cover patterns due to its repetitive data acquisition and availability of accurate geo-referencing procedures.[22]

The spatiotemporal density and extent of land cover vary with agro-climatic zones, slope, and soil type. In the past, land use changes were marginal in the study area where land use planning was least imperative,[23] whereas in recent times, progressive land degradation and unplanned utilization of land resources is seriously aggravating the incidence of poverty and food insecurity. This proves the importance of time series analysis of land cover change pattern in the area characterized by 2 dominant physiographic units: highland escarpments and high plateaus.

Land use land cover study is essential in describing the way the land is currently used and provides a starting point for present and future planning. To this end, acquiring reliable and updated spatiotemporal information on land cover change requires formulating systematic methods, tools, and techniques.[24] The main objective of this study was to assess the long-term spatiotemporal land cover change patterns, and the specific objectives of the research were to quantify the rate, trend, and magnitude of change with topography for the selection, planning, and implementation of development strategies. To achieve these objectives, we used rich archive and spectral resolution Landsat data sets, the Bayesian ML-supervised classifier to map the land use class, and change detection comparison techniques to identify intra-image land cover change.[25]

Materials and Methods

Area description

The study area is located on the eastern border of Amhara Regional State, east of the capital Addis Ababa, following the water-dividing ridge containing Awash and Afar-Danakil basins. The area (18 772.78 km^2) with an eastern orientation is geographically located between 8.5° and 12.5° north (Figure 1) and 39° and 40.5° east. The elevation of the area ranges from 580 to 3960 m (above mean sea level). Numerous rivers originated from western highlands flow towards the eastern lowlands of Denakil plain and Awash River basins. The area contains a number of discrete catchments and sub-catchments that carry run-off from uplands draining the region's periphery into 4 major river basins: Abbay, Tekezé, Awash, and Afar-Danakil basins.

The climate of the region is largely controlled by distinct dry and wet seasons with unimodal rainfall distribution and pronounced wetter and drier cycles that vary considerably from year to year. The rainy season extends from June to September receiving nearly 70% to 90% of the annual rainfall.[26,27] The mean annual rainfall ranges from 476 to 1930 mm. The mean annual temperature varies from place to place classifying the area into 4 traditional, agroecological zones, Wurch (<14°C), Dega (14°C-18°C), Weyna Dega (18°C-20°C), and Kolla (18°C-24°C), that account nearly 1%, 16%, 46%, and 37% of the area, respectively.[28,29]

The most common classification specific to agriculture (Figure S1, left) uses agro-climatic zones which applies the

water balance concept and the length of the growing season including the onset dates at certain probability levels.[30] The water balance concept classifies the region into 3 distinct zones, namely, areas without a significant growing period (N), areas with a single growing period (S), and areas with a double growing period (D). However, the classification based on agroecological zonation, the spatial classification of the landscape into area units with similar agricultural and ecological characteristics, is shown in the agroecological belt model (Figure S1, right) as extrapolated from agro-climatic regions.[31] In general, climate study and classification is rather complex that has been the topic of many studies.[32]

Materials

Selection of the most appropriate RS image considers different factors such as complexity of the area, coverage, and level of spatial detail required for the specific objective. Remote sensing–based change detection analysis uses time series multi-date (multi-sensor) images to evaluate land cover change under natural and human alterations.[23] In this research, 5 multi-temporal cloud-free Landsat TM images (path 168 and rows 52-54) covering the period 1995 to 2014 were used. The data captured on February were provided by the National Aeronautics and Space Administration (NASA)/US Geological Survey (USGS).

To analyse the trend and magnitude of land use change, we used time series 30-m resolution TM Landsat images and 1:50 000-scale topographic maps acquired from the Ethiopian Mapping Agency to georeference the satellite image and extract essential features related to the area. A 30-m resolution Advanced Spaceborne Thermal Emission and Reflection Radiometer (ASTER) Global Digital Elevation Model (GDEM) was used as a principal material to generate contour, slope maps, and as auxiliary data to support the accuracy of image classification. The GDEM was acquired from the Earth Remote Sensing Data Analysis Center (ERSDAC) of Japan and NASA's Land Processes Distributed Active Archive Center (LPDAAC).[33] To process the resulting data, we have used the Earth Resources Data Analysis System (ERDAS IMAGINE 2013), ArcGIS10.3, and Environment for Visualizing Images (ENVI 4.7). Quantitative analysis of spatial and historical land cover changes was analysed by subtraction of images of the same location using GIS and RS tools that provide a flexible environment for collecting, storing, displaying, and analysing digital data necessary for change detection.[34] The effect of topography on each of the data types and classification methods in terms of geometric properties and thematic accuracy was improved using auxiliary terrain data sets.

Methodology

The methodology and procedure employed in the LULC study included interpretation and analysis of recent and middle-aged satellite images, normalized difference vegetation index (NDVI) and NDVI differencing (DNDVI) analysis, preliminary land use and land cover classification and mapping, field and signature data collection and verification, and post land cover mapping (Figure 2). During pre-fieldwork, the images were rectified and enhanced to create a more realistic representation of the scene and land cover signatures. Geospatial data uncertainty resulted from image resampling, percent cloud cover, assumptions of homogeneity, and physical properties of feature of interest were improved by applying geometric and radiometric corrections.[35,36] Nearest neighbour resampling method was employed and colour balance or contrast stretching was used for image enhancement through histogram equalization.[37]

Image pre-processing. Image processing involves manipulation and interpretation of digital images. The spatial resolution of images was enhanced using resolution merge technique that integrates images of different spatial resolution or pixels. Radiometric enhancement, however, improved the area image classification by addressing stripping and banding errors that occur when the detector goes out of adjustment.[7,38] In addition, principal component analysis improved the image visualization with a technique of data compression to produce uncorrelated output bands, segregate noise components, and reduce the dimensionality of data sets.[39]

During image pre-processing, TM digital images of varying resolution were resampled for spatiospectral resolution, layer stacked for the different scenes, and geometrically transformed. Geometric transformation of digital images modifies the spatial relationship between pixels in an image for post-processing. Image resampling involves the conversion of satellite imagery at a relatively fine scale to a more coarse spatial resolution with imagery from similar or different satellite sensors with varying spatial resolution. The choice of the resampling method depends, among others, on the ratio between input and output pixel sizes and the purpose of the resampled image.[40] In this research, Landsat TM images were resampled using the nearest neighbour resampling technique to preserve the original image radiometric information.[41] In addition, nearest neighbour assigns the digital number, value of the closest original pixel to the new pixel by retaining all spectral information for efficient image classification.[40,42]

Classification and land cover mapping

Various classification methods have been developed to extract essential information from imageries. The 2 main types used in this research were the pixel and object-based classification techniques. Pixel-based methods can be cluster-based unsupervised or supervised classification,[43] whereas the later uses statistical (eg, ML) and non-statistical (eg, support vector machines) algorithms.[44] The object-based classification which overcomes some of the particular problems encountered with pixel-based classification[45] was used to analyse all the spatiotemporal TM data sets.

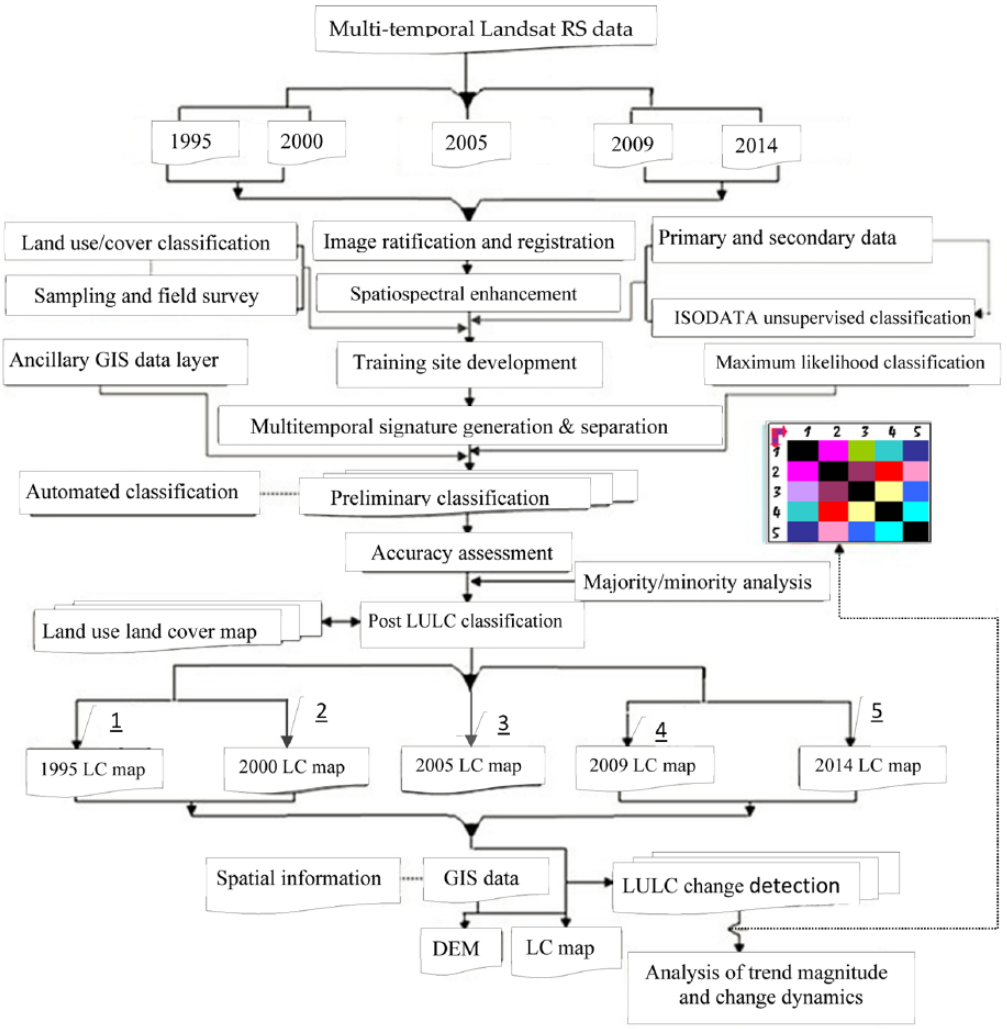

Figure 2. A flow diagram for LULC mapping and change detection analysis modified from Ayele et al.[7]

Image data were first classified by aggregating images into natural groupings or clusters present in the scene based on their inherent spectral properties. The false colour composite unsupervised land cover classification maps (Figure 3) were prepared using the ISODATA (Iterative Self-Organizing Data Analysis) clustering algorithm.[46] During RS image classification and interpretations, field and local area knowledge of land cover types and patterns were used as training site development for the supervised classification. Following the supervised image classification, change detection analysis was made to quantify the rate, magnitude, and pattern of land cover change.[47] The most common satellite image classification algorithms applied in this study is the ML classifier that touches a probability density function and guesses the probability with which a specific pixel belongs to a specific class. Larger deviations from the centre point will be allowed where a pixel is not in the area of a contesting category.[39] The ML-supervised classification techniques work with Bayes theorem and uses a discriminant function to assign the pixel to the class with the highest probability.[48] Each image pixel belongs to the land cover class for which they have the highest membership likelihood following the Gaussian normal distribution function.[18] Although the ML classifier is slow in computation and sometimes unsafe in assuming Gaussian-distributed input data classes, yet, it is a more accurate statistical decision criterion in classifying overlapping signatures. The ML-supervised classification derived from the Bayes theorem is given as follows:

$$P(i\,|\,\omega) = \frac{P(\omega\,|\,i)P(i)}{P(\omega)} \tag{1}$$

where $P(i\,|\,\omega)$ is the likelihood function, a posteriori distribution, ie, the probability that a pixel with feature vector ω belongs to class I; $P(i)$ is the priori information, ie, the probability that class i occurs in the study area and $P(\omega)$ is the probability that ω is observed. $P(\omega)$ can be written as follows:

$$P(\omega) = \sum_{i=1}^{m} P(\omega\,|\,i)P(i) \tag{2}$$

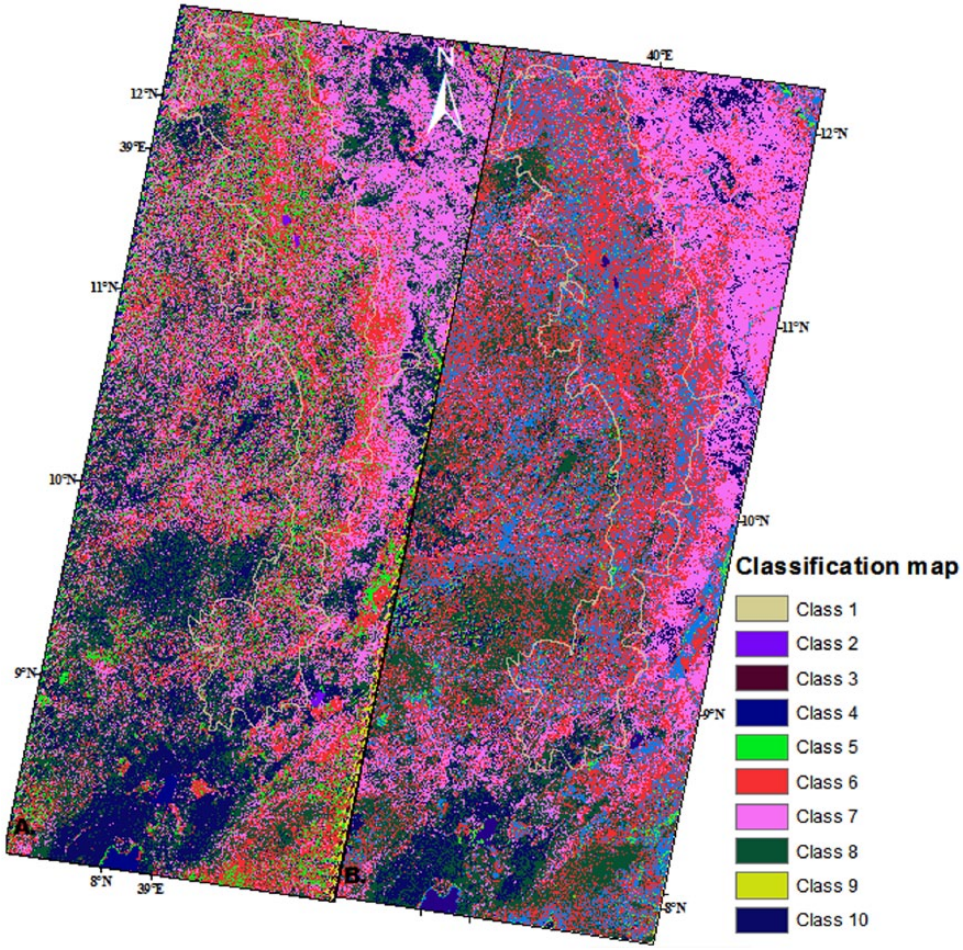

Figure 3. Comparative 10-class ISODATA unsupervised classification map for Landsat images: (A) 2005 and (B) 2009.

where M is the number of classes. $P(\omega)$ is a normalization constant to ensure that $P(i|\omega)$ sums to 1. Any pixel x is assigned to class i by the following rule:

$$x \in i \text{ if } P(i|\omega) > P(j|\omega) \text{ for all } j \neq i \quad (3)$$

Maximum likelihood often assumes that the distribution of the data within a given class i obeys a multivariate Gaussian distribution. The discriminant or monotonic log-likelihood function[48,49]; function is then define as follows:

$$g_{(i)}(\omega) = \ln p(\omega|i) = -1/2(\omega-\mu_i)^i C_i^{-1}(\omega-\mu_i) - N/2\ln(2\Pi) - 1/2\ln(|C_i|) \quad (4)$$

Each pixel is assigned to the class with the highest likelihood or labelled as unclassified if the probability values are all below a user-defined threshold.[18]

Post-classification change detection. Following image pre-processing, image post-processing and LULC classification were defined according to the classification schemes in Food and Agriculture Organization (FAO) guides[50] where land use and land cover of the area were mapped using vegetation cover, type, and intensity of cultivation. The topographic map of the study area printed at 1:50 000 scales was used as an important resource to georeference the image and extract essential features related to each land use and land cover unit.

Results and Discussion

The LULC maps produced from object-based classifications were assessed for their accuracy. For the object-based classification that uses the ML classifier, we used more than 283 random, well-distributed field samples for training site development. To make image reinterpretation and analysis reliable and relatively homogeneous, representative attribute data and land cover signatures were collected using the ISODATA false colour unsupervised classification map as a field guide (Figure 3). Image post-classification error matrix was computed as the total number of correct class predictions divided by total number of cells,[51] and the accuracy of classification was assessed using contingency table (confusion or error matrix) produced from a random sample of individual pixels or clusters compared with known cover conditions over the same pixel areas.[52]

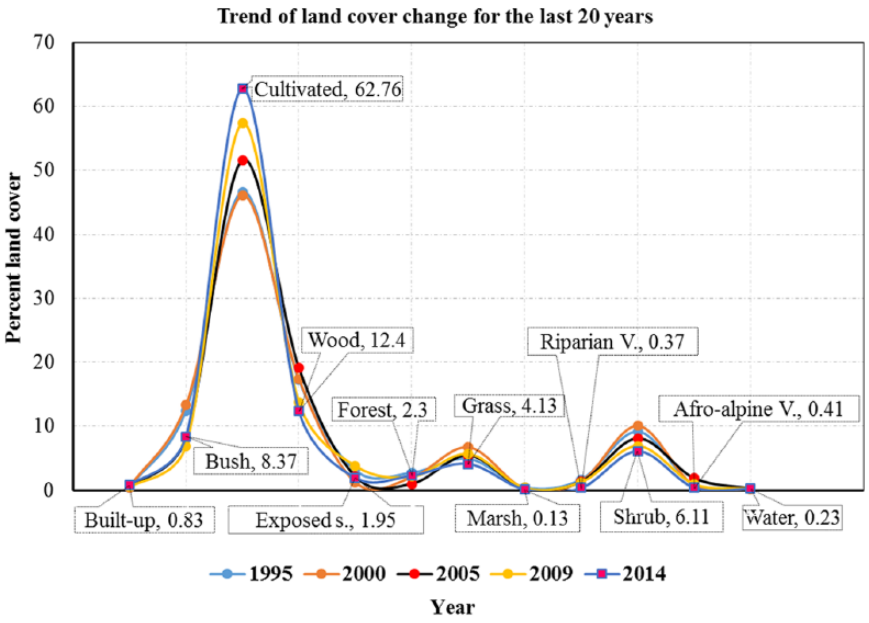

Figure 4. Trend and magnitude of land cover change for the past 20 years: a call-out map for the 2014 land cover distribution.

LULC classification

Remote sensing images were analysed using object-based supervised ML classification algorism that uses the means and variances of the training data to estimate the probability that a pixel is a member of a class. In ML, the pixel which is placed in the class has the highest probability of membership.[53] A classification scheme was developed for further analysis of the images, based on the characteristics and land cover types of the area (Table 2).

The final Bayesian ML classification resulted in 12 major land cover units and 43 subunits with automatic merging of closer values of reflectance properties and characteristics (Table S1). The ML-supervised classification of the 2014 Landsat TM image revealed that most of the area was covered by cultivated, wood, bush, shrub, grass, and forest land mapping units accounting 62.8%, 12.4%, 8.4%, 6.1%, 4.1%, and 2.4% of the total, respectively. However, exposed surface, built-up area, afro-alpine vegetation, riparian vegetation, water body, and marsh areas covered only small portion of the land area (Figure 4). Details of land use unit areas and subunits for the 2014 image analysis can be found in the supplementary table (Table S1).

Trend of LULC change. The trend and magnitude of land cover change were analysed for a period of 5 and 10 years from the benchmark year, 1995. The bidecadal trend of land cover change revealed that there was a major increase in the cultivated land that can be represented by an exponential growth model (Table 1, Figure S2). Cultivated land was expanding at the expense of the remaining land units as explained in the tabular trend models. The degree of expansion was shown with 93% strong positive correlation coefficient, where Y is the forecast and t is a variable time value. In this study, the general trend of built-up areas has shown an increasing trend due to population expansion and its demand for infrastructure development. The result of bidecadal trend analysis revealed that built-up areas covered 0.47%, 0.49%, 0.56%, 0.52%, and 0.83% of the total area for increasing order of the analysis years (Table 2). The highest share of built-up areas is found near the urban cities and homesteads.

On the contrary, the trend of 5 years–based LULC change detection analysis for exposed surfaces, grassland, afro-alpine vegetation, and water body was less predicted with exponential models. As a result, we used polynomial model approximations as explained by the statistical significance test, R^2 values. The statistical efficiency criterion, R^2 values more than 0.7, showed reasonably good agreement between the dependent and the independent variables and a value above 0.6 is also acceptable.

LULC change detection. Change detection involves the use of multispectral data sets to discriminate area of land cover change between dates of imaging. Change detection procedures included analysis of sensor data, spatial resolution, viewing geometry, spectral bands, radiometric resolution, and the time of day. Following image pre-processing, multi-temporal TM images were post-processed to quantify the area of change and change rate, the spatial distribution of change types, change trajectories, and accuracy assessment of change detection results.

Two change detection techniques, pre- and post-classification were used for the length of the records. The former method analyses the change using the NDVI[54] and the latter and the most widely used change detection method uses the ML classification algorism. Post-classification evaluates the change in LULC based on a detail-categorized classification of land cover units.

Table 1. Best fit models to analyse the trend of land use land cover change dynamics.

LAND USE UNIT	BEST FIT MODEL EQUATION	STATISTICAL EFFICIENCY, R^2 (%)	TREND MODEL
Built-up	$Y=0.4e^{0.1197t}$	69	Exponential growth
Bushland	$Y=14.7e^{-0.144t}$	64	Exponential decay
Cultivated land	$Y=41.2e^{0.0812t}$	93	Exponential growth
Woodland	$Y=20.7e^{-0.09t}$	61	Exponential decay
Exposed surface	$Y=-0.52t^3+4.8t^2-12.6t+11.6$	98	Third-order polynomial
Forest cover	$Y=-0.06t^3+0.82t^2-3.2t+5.2$	76	Third-order polynomial
Grassland	$Y=-0.37t^2+1.96t+3.6$	72	Second-order polynomial
Marshland	$Y=0.55e^{-0.227t}$	53	Exponential decay
Riparian vegetation	$Y=2.8e^{-0.314t}$	65	Exponential decay
Shrubland	$Y=11.4e^{-0.119t}$	86	Exponential decay
Afro-alpine vegetation	$Y=-0.07t^3+0.4t^2-0.35t+0.72$	63	Third-order polynomial
Water body	$Y=-0.01t^3+0.1t^2-0.18t+0.5$	89	Third-order polynomial

Y is the percent coverage of land cover unit after time *t* (years).
These results are based on 5 multi-temporal cloud-free Landsat Thematic Mapper images to represent the trend of land cover change for the past 2 decades. However, the fit equation and the corresponding trend may vary with image spatiotemporal resolution, required level of spatial detailing, human activity, and unpredicted climate change.

Table 2. Land cover distribution in hectares and percent coverage of 12 major land cover units from 1995 to 2014.

AREA, HECTARES AND % COVERAGE										
LAND COVER	1995	% COVER	2000	% COVER	2005	% COVER	2009	% COVER	2014	% COVER
Built-up	8898	0.47	9244	0.49	10463	0.56	9698	0.52	15664	0.83
Bushland	233507	12.44	249645	13.30	151850	8.09	130357	6.94	157186	8.37
Cultivated land	876176	46.67	864102	46.03	969049	51.62	1076798	57.36	1178098	62.76
Woodland	324022	17.26	327680	17.46	359627	19.16	257436	13.71	232694	12.40
Exposed surface	58561	3.12	23591	1.26	40950	2.18	71727	3.82	36666	1.95
Forest land	51430	2.74	37212	1.98	19182	1.02	39711	2.12	43258	2.30
Grassland	92882	4.95	126543	6.74	102581	5.46	106900	5.69	77500	4.13
Marshland	8759	0.47	5195	0.28	4636	0.25	7065	0.38	2456	0.13
Riparian vegetation	31477	1.68	26898	1.43	25661	1.37	23968	1.28	6962	0.37
Shrubland	172439	9.19	189110	10.07	152690	8.13	130356	6.94	114788	6.11
Afro-alpine vegetation	14641	0.78	13949	0.74	35515	1.89	18260	0.97	7756	0.41
Water body	4486	0.24	4109	0.22	5074	0.27	5002	0.27	4250	0.23
Total	1877278	100	1877278	100	1877278	100	1877278	100	1877278	100

Pre-classification change detection. The NDVI is a function of 2 bands: the red and near-infrared spectral band.[55] The NDVI is calculated on a per-pixel basis as the normalized difference between near-infrared and red bands given as follows:

$$NDVI = \frac{NIR - RED}{NIR + RED} \quad (5)$$

where *NIR* and *RED* are the near-infrared and red band values, respectively, for the cell. The classification maps for the years 2005 and 2009 are shown in Figure 5 (bottom).

Landsat TM data of all dates were independently classified based on the NDVI value that ranges from –1 to +1. The NDVI values were further modified by employing histogram equalization enhancement which results in equal probability range of 0 to 255 for both images. Water bodies which reflect more in the visible band than in the near-infrared band appear to have negative NDVI values, whereas bare soil and rocks have NDVI value of around 0. Negative NDVI values mapped darker indicated features that reflect more in the visible band than in the near-infrared band. This in turn indicated areas of low vegetation density, typical water, cloud, bare soil, and rock.[18]

Healthy green vegetation, however, has stronger near-infrared reflectance thereby providing NDVI values close to +1.[56] From the result, NDVI value ranging from 0.2 to 1 can represent the vegetation density from sparse to dense vegetation canopy. The grey-scale NDVI map (Figure 5, top) is presented for visual simplicity and to spatially cross-reference the distribution and extent of different land cover units.

NDVI differencing. The vegetation indices differencing, DNDVI, approach was used to measure the change in biomass between initial and final state NDVI images. This method statisticizes and compares NDVI values between images acquired on 2 different dates. Prior to applying NDVI image differencing, the individual NDVI images of each date were generated with a range of values from –1 for water to +1 for dense vegetation canopy. The DNDVI is then created through the subtraction of 2 different time period NDVI images. Equation 6 shows the DNDVI between 2005 and 2009. In this case, 2009 is the final state image and 2005 is the initial image:

$$DNDVI = NDVI(2009) - NDVI(2000) \quad (6)$$

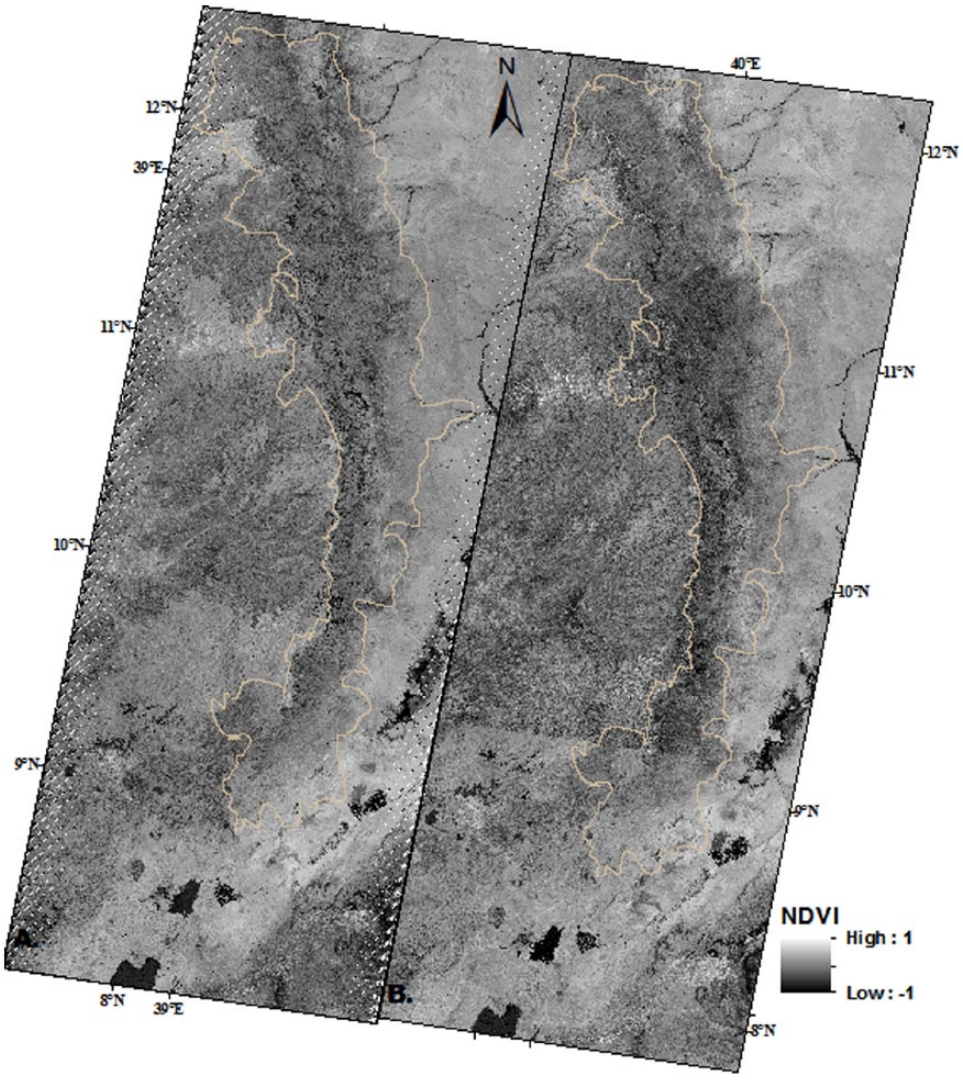

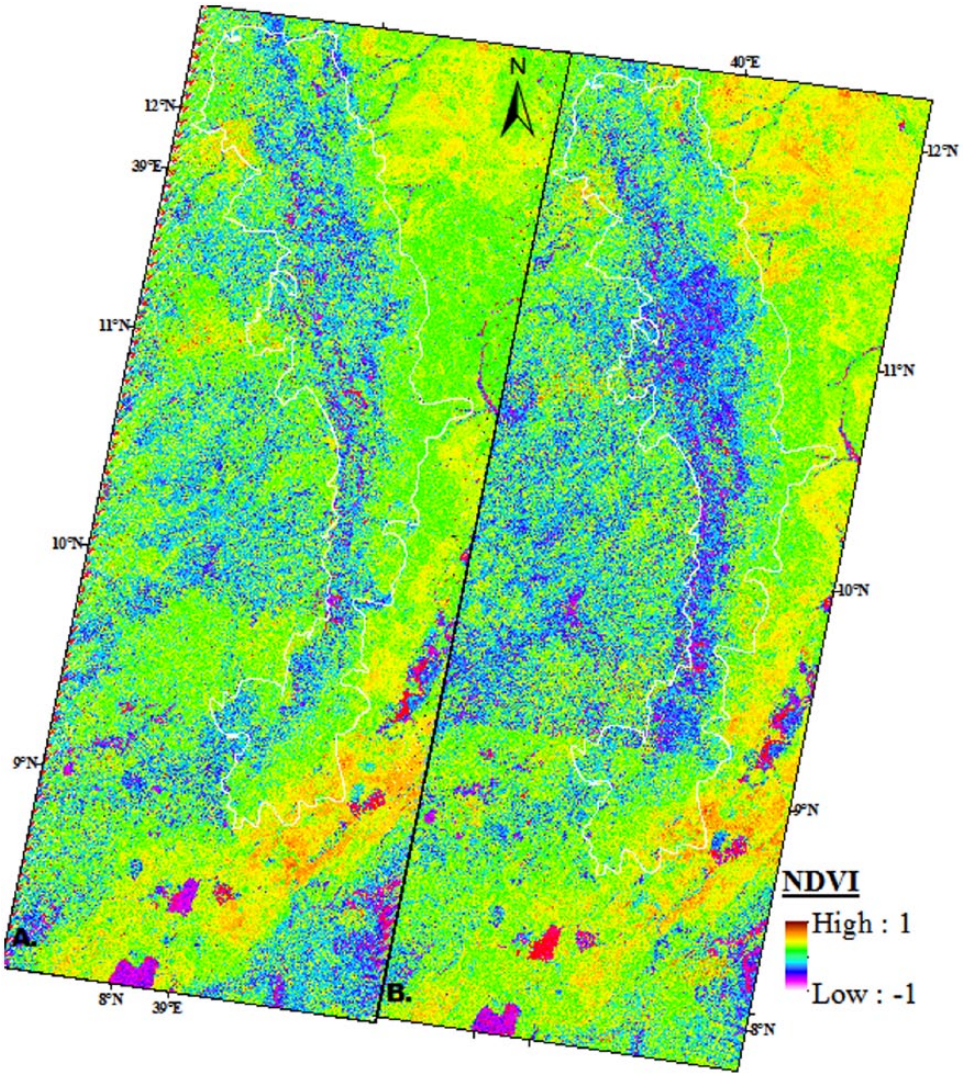

Figure 5. NDVI maps for (A) 2005 (left) and (B) 2009 (right): grey-scale representation (top). Colour representation (bottom) of bidecadal NDVI values for (A) 2005 and (B) 2009.

Following the pre-NDVI processing and image enhancement, the bidecadal changes in the land/vegetation cover can be inferred. In the DNDVI image (Figure 6B), land cover units that have experienced changes are assigned with red and blue colours. The gain in vegetation during the bidecadal analysis is represented by the flame red colour. Similarly, dark blue areas represent land covers that have lost vegetation. The grey-scale DNDVI map is presented for visual simplicity and spatial cross reference. The major increase in NDVI values between 2005 and 2009 is in the agricultural areas at the expense of bush, shrub, and woodland units (Figure 7, Table 3). The overall trend of the vegetation cover change can also be found under post-classification change detection.

Post-classification change detection. For a detailed analysis of the spatiotemporal change dynamics, we employed an object-based supervised classification technique that uses the Bayesian ML algorithm. Ground truth data obtained from aerial images and training sites were used in the ML classification. Post-classification comparison approach was used to analyse the LULC change between initial and final state images.

The trend and rate of major land cover changes were analysed using time series Landsat TM digital images from 1995 to 2014 (Figure 7). To quantify the trend, rate, and magnitude of change between 2 images, we used a time interval of 5 and 10 years from the benchmark, 1995. As shown in the tabular detail, the dominant land use types in the area were agricultural and woodland units, which covered nearly 63.9%, 63.5%, 70.8%, 71.1%, and 75.2% of the entire area for the years 1995, 2000, 2005, 2009, and 2014, respectively (Table 3). Land cover change with agro-climatic zones, soil types, and slope classes was common in most part of the area, and the conversion of grazing land into plantation trees and closure area development were major changes in the past 20 years. The significant factors for land cover changes during these periods were attributed to population growth and its demand for additional

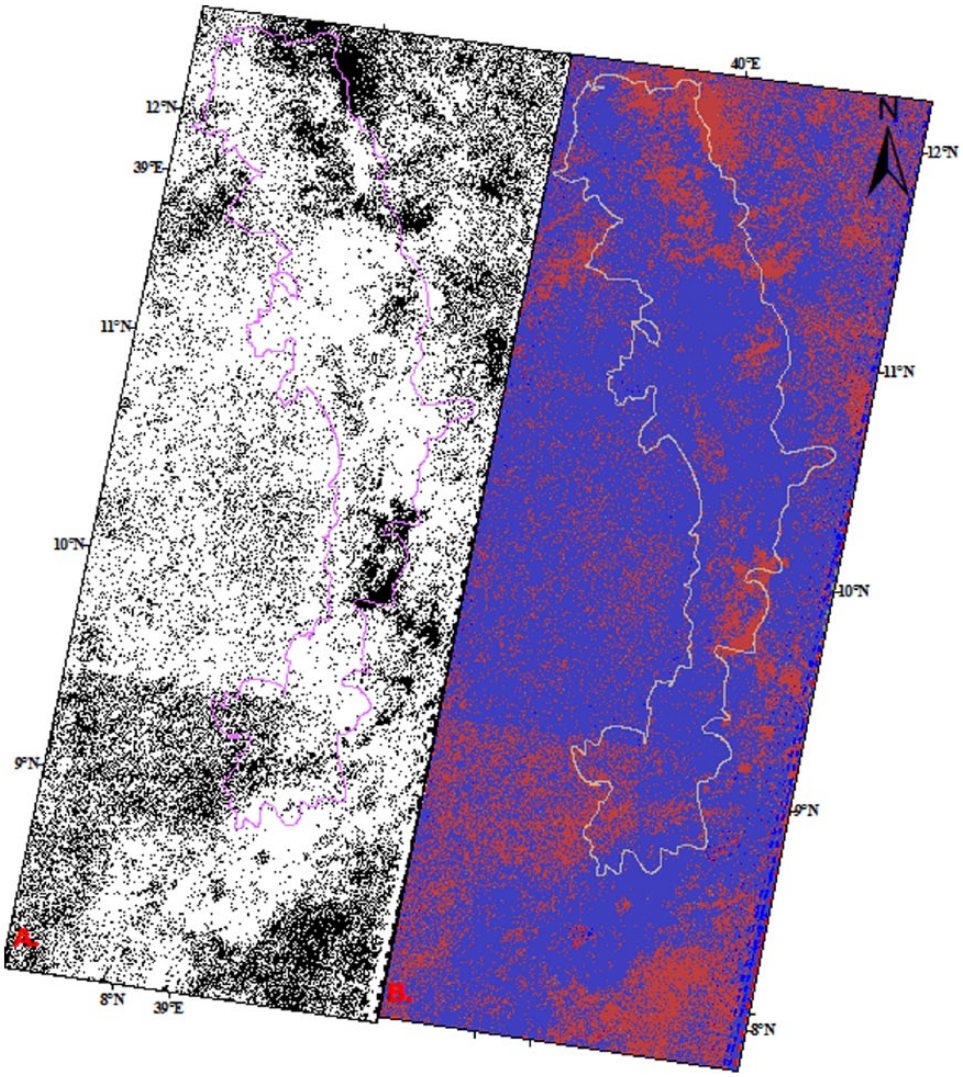

Figure 6. DNDVI-based land cover change detection for the year (A) 2005 and (B) 2009.

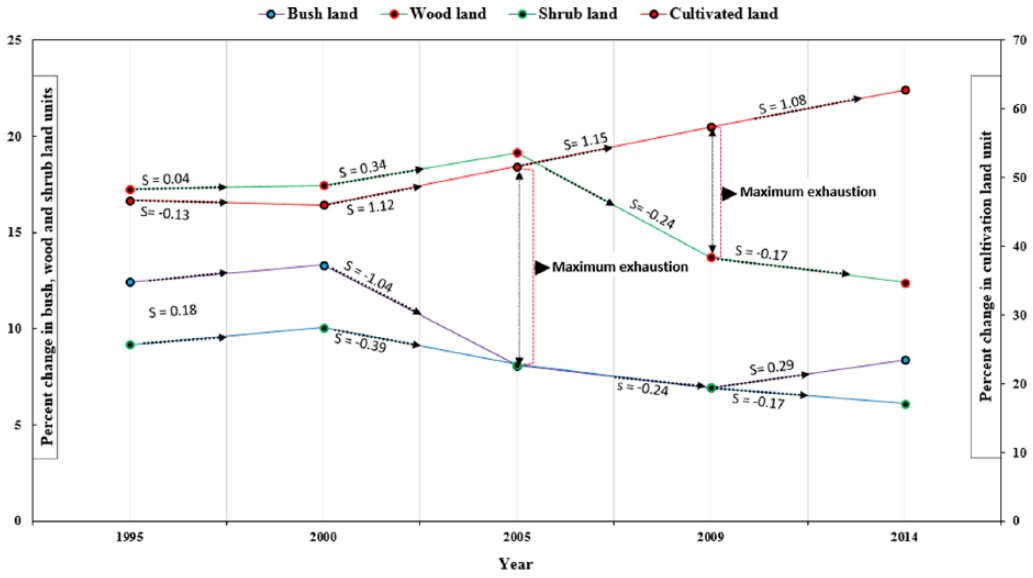

Figure 7. Trend, rate, and magnitude of land cover change for the major land cover units.

Table 3. Post-classification change detection matrix for the past 20 years from 5 cloud-free Landsat Thematic Mapper images, 1995 to 2014.

LAND COVER UNIT	% AREA COVER		CHANGE		% AREA COVER		CHANGE		% AREA COVER		CHANGE	
	1995	2000	%	SPEED,%	2000	2005	%	SPEED,%	2005	2009	%	SPEED, %
Built-up	0.47	0.49	0.02	0.004	0.49	0.56	0.06	0.013	0.56	0.52	−0.04	−0.008
Bushland	12.44	13.3	0.86	0.172	13.3	8.09	−5.21	−1.042	8.09	6.94	−1.14	−0.229
Cultivated land	46.67	46.03	−0.64	−0.129	46.03	51.62	5.59	1.118	51.62	57.36	5.74	1.148
Woodland	17.26	17.5	0.19	0.039	17.46	19.16	1.7	0.34	19.16	13.7	−5.44	−−1.089
Exposed surface	3.12	1.26	−1.86	−0.373	1.26	2.18	0.92	0.185	2.18	3.82	1.64	0.328
Forest land	2.74	1.98	−0.76	−0.151	1.98	1.02	−0.96	−0.192	1.02	2.12	1.09	0.219
Grassland	4.95	6.74	1.79	0.359	6.74	5.46	−1.28	−0.255	5.46	5.69	0.23	0.046
Marshland	0.47	0.28	−0.19	−0.038	0.28	0.25	−0.03	−0.006	0.25	0.38	0.13	0.026
Riparian vegetation	1.68	1.43	−0.24	−0.049	1.43	1.37	−0.07	v0.013	1.37	1.28	−0.09	−0.018
Shrubland	9.19	10.1	0.89	0.178	10.07	8.13	−1.94	−0.388	8.13	6.94	−1.19	−0.238
Afro-alpine vegetation	0.78	0.74	−0.04	−0.007	0.74	1.89	1.15	0.23	1.89	0.97	v0.92	−0.184
Water body	0.24	0.22	−0.02	−0.004	0.22	0.27	0.05	0.01	0.27	0.27	0	−0.001
Total	100	100	0.0	0.0	100	100	0.0	0.0	100	100	0.0	0.0
LAND COVER UNIT	% AREA COVER		CHANGE		% AREA COVER		CHANGE		% AREA COVER		CHANGE	
	2009	2014	%	SPEED, %	1995	2005	%	SPEED, %	2005	2014	%	SPEED, %
Built-up	0.52	0.83	0.32	0.064	0.47	0.56	0.08	0.008	0.56	0.83	0.28	0.028
Bushland	6.94	8.37	1.43	0.286	12.44	8.09	−4.35	−0.435	8.09	8.37	0.28	0.028
Cultivated land	57.36	62.8	5.4	1.079	46.67	51.6	4.95	0.495	51.62	62.8	11.14	1.114
Woodland	13.71	12.4	−1.32	−0.264	17.26	19.2	1.9	0.19	19.16	12.4	−6.76	−0.676
Exposed surface	3.82	1.95	−1.87	−0.374	3.12	2.18	−0.94	−0.094	2.18	1.95	−0.23	−0.023
Forest land	2.12	2.3	0.19	0.038	2.74	1.02	−1.72	−0.172	1.02	2.3	1.28	0.128
Grassland	5.69	4.13	−1.57	−0.313	4.95	5.46	0.52	0.052	5.46	4.13	−1.34	−0.134
Marshland	0.38	0.13	−0.25	−0.049	0.47	0.25	−0.22	−0.022	0.25	0.13	−0.12	−0.012
Riparian vegetation	1.28	0.37	−0.91	−0.181	1.68	1.37	−0.31	−0.031	1.37	0.37	−1	−0.1
Shrubland	6.94	6.11	−0.83	−0.166	9.19	8.13	−1.05	−0.105	8.13	6.11	−2.02	−0.202
Afro-alpine vegetation	0.97	0.41	−0.56	−0.112	0.78	1.89	1.11	0.111	1.89	0.41	−1.48	−0.148
Water body	0.27	0.23	−0.04	−0.008	0.24	0.27	0.03	0.003	0.27	0.23	−0.04	−0.004
Total	100	100	0.0	0.0	100	100	0.0	0.0	100	100	0.0	0.0

cultivable land, land degradation on steep and hilltop slopes, poor land management, rising demand for cash crops, partial implementation of policy strategies, and loose land and resources administration.

The post-classification matrix (Table 3) shows the individual class percentage and change statistics for 5 cloud-free multi-temporal Landsat TM images. The percent land cover distribution, percent change in the areal extent of each land

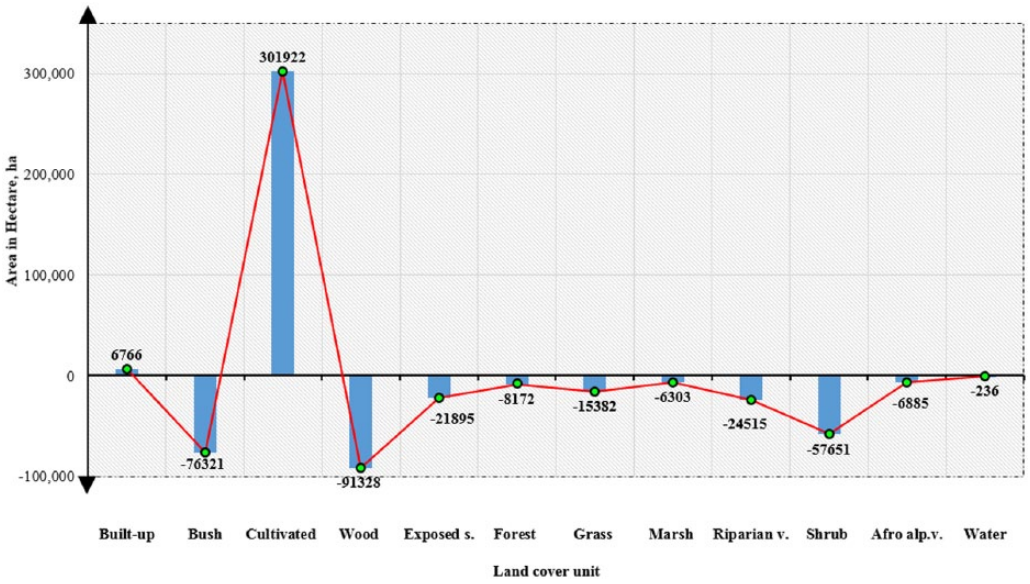

Figure 8. Land use land cover change between 1995 and 2014.

cover unit between initial and final state images, and rate of change expressed as the slope of the line, and the time rate of change of final and initial state images are clearly presented in the table. In addition, the total land use unit areas, percentage coverage, and corresponding area ratio are indicated in Table 2. The tabular figure is self-explanatory to analyse the change statistics for the 12 major land cover units considered.

From Table 3, it can be observed that the cultivated land unit is continuously increasing with a significantly higher positive slope at the expense of the other land use units (Figure 7). The largest increase was shown between 2005 and 2009 that covered above 107 750 hectares (5.74%) of the total study area. However, there was a slight decrease in cultivated land, decay slope of 0.13, between the years 1995 and 2000. This was mainly due to the significant increase in some major land cover units, such as bush, shrub, and woodland. Built-up areas showed a steady increase excepting the year 2009, where the spatial extent has reduced by 765 hectares from the previous.

Between the years 2005 and 2009, there was a drastic decrease in the woodland unit amounting 102 191 hectares of land. This was the maximum exhaustion covering nearly 5.5% of the entire area (Figure 7). The next highest change was observed between the years 2000 and 2005 for the bushland unit. According to the statistics, the bushland showed a sudden decrease covering 97 795 hectares, 5.2% of the area. There were also moderate decreased in shrubland units between 2000 and 2005 that covered 36 420 hectares (1.94%) of the entire area. The remaining land cover units showed a general decrease (riparian vegetation) and some showed a fluctuating trend (eg, exposed surface, forest, and marshland units). The riparian vegetation has shown a steady decrease throughout the analysis period except for the year 2014, where there was a maximum decline from the previous percent coverage.

The area of water bodies remained nearly constant with a changing slope significantly less than ±0.01%. The only highest outliers were observed between 2005 (0.27%) and 2009 (0.27%), change slope of 0%, which covered 506 865 hectares of the total area. Similarly, in 2005, there was a substantial increase in the afro-alpine vegetation covering nearly 2% of the entire area. The forest coverage that showed a rapid decline (1%) between 2000 and 2005 later showed a drastic increase (1.1%) between 2005 and 2009. The area remained nearly constant for the year 2014. Comparing the change statistics from 2000 to 2005 and 2005 to 2009, it can be seen that the rate of change of forest coverage was about −0.2% and 0.22%, respectively (Table 3). Results revealed that there was a general increase for cultivated and built-up areas and a decrease for riparian vegetation.

Image differencing for LULC change detection. Image differencing is among the numerous methods that have been developed and used for LULC change detection.[57] Image difference, the difference in the total number of equivalently classed pixels between 2 images, is computed by subtracting the initial state class totals from the final state class totals. The image difference change detection statistics between 1995 and 2014 (Figure 8) details the magnitude of land cover charge for the past 2 decades. A positive value of image difference indicates an increase in class size and a decrease in class size is represented by a negative value. Cultivated land (+301 922 hectares) and built-up (6766 hectares) showed an increase in the spatial neighbourhood. The remaining 10 land use units, namely, bush (−76 321), wood (−91 328), exposed surface (−21 895), forest (−8172), grass (−15 382), marsh (−6303), riparian vegetation (−24 515), shrub (−57 651), afro-alpine vegetation (−6885), and water body (−236), were contributing to the cultivated and built-up areas. In other words, in the year 2014, the areal extent of cultivated and built-up areas was increased by 301 922 and 6766 hectares,

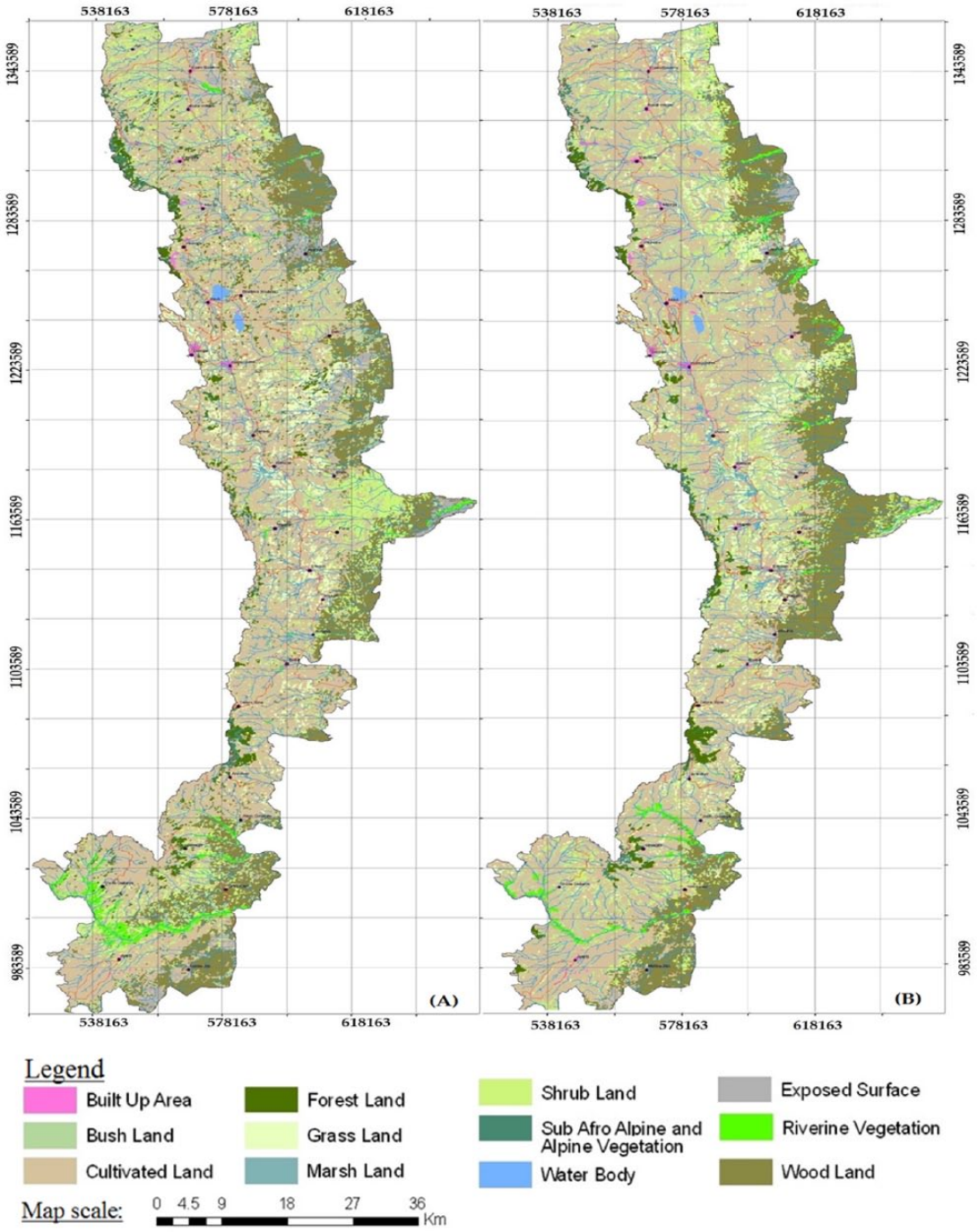

Figure 9. Land cover map: (A) 1995 and (B) 2000.

respectively, at the expense of the other land use units labelled by negative values.

In general, the area undergoes a radical change in its form from 1995 to 2014, 2 decades. Both pre- and post-classification change detection approaches were used to assess the change, and Landsat TM satellite images were used for detail analysis from USGS satellite data archive. Figures 9 to 11 compare 5 land cover maps for the years 1995, 2000, 2005, 2009, and 2014. The colour figures are self-explanatory to analyse the time response of each land cover unit. The post-classification change detection analysis (Table 3) is the numeric representation of these land cover maps. We used the ML classifier to create the signature class of significant land cover category and PCC analysis to assess the change dynamics. Image differencing and statistical change detection techniques were used to quantify the spatial coverage of the different land use units for the year 2014 (Figure 8).

Land use change with slope gradient

Continuously increasing demand of land for agriculture over decades had brought about changes in the land cover and

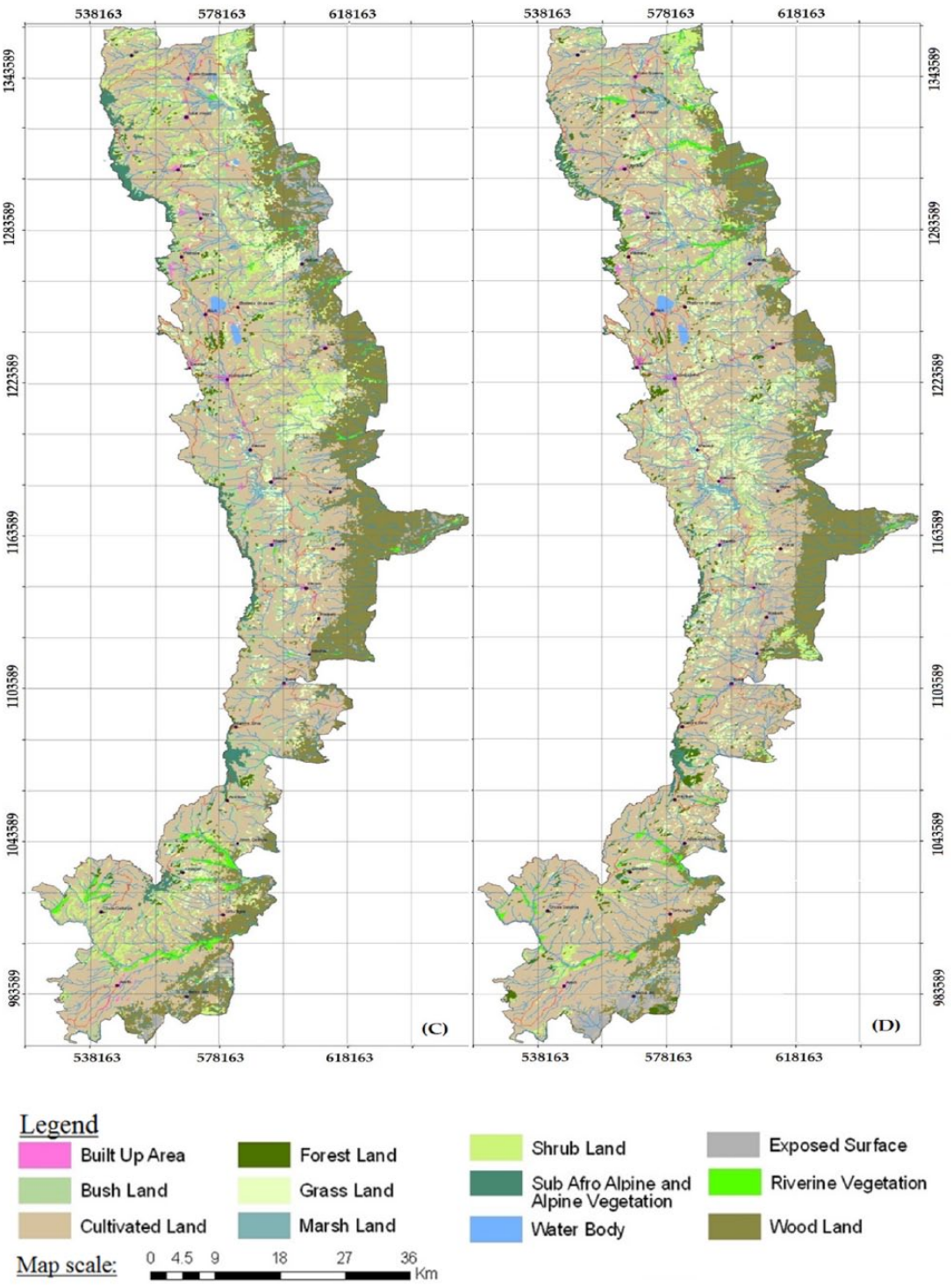

Figure 10. Land cover map: (C) 2005 and (D) 2009.

deforestation of higher slope areas. Cultivated land cover in the study area expanded substantially to the higher slopes whenever agriculture was possible. Table 4 shows the spatial distribution of land cover with terrain slope. The highest percentage of land coverage, 674 826 hectares (35.9%) of land, was found in the slope ranging from 30% to 60% and the next higher value, covering 489 021 hectares (26%) lied under the 15% to 30% slope range. The cultivated land unit covered nearly 18% and 22% of the total land cover for terrain slopes ranging from 15% to 30% and 30% to 60%, respectively. However, the percent coverage of cultivated land dropped to 1.6% of the total (4.1%) for agriculturally inaccessible slopes (slope >60%). For terrain slopes between 0% to 2% and 5% to 8%, nearly half the total slope area, 0.5% of 1.1% and 2.1% of 2.9%, respectively, was covered by cultivated land. The remaining half percentage was represented by the other 11 land cover units.

The next higher proportion of the area was covered by woodland making nearly 0.1%, 2.1%, 0.4%, 3.5%, 3.8%, 2.5%,

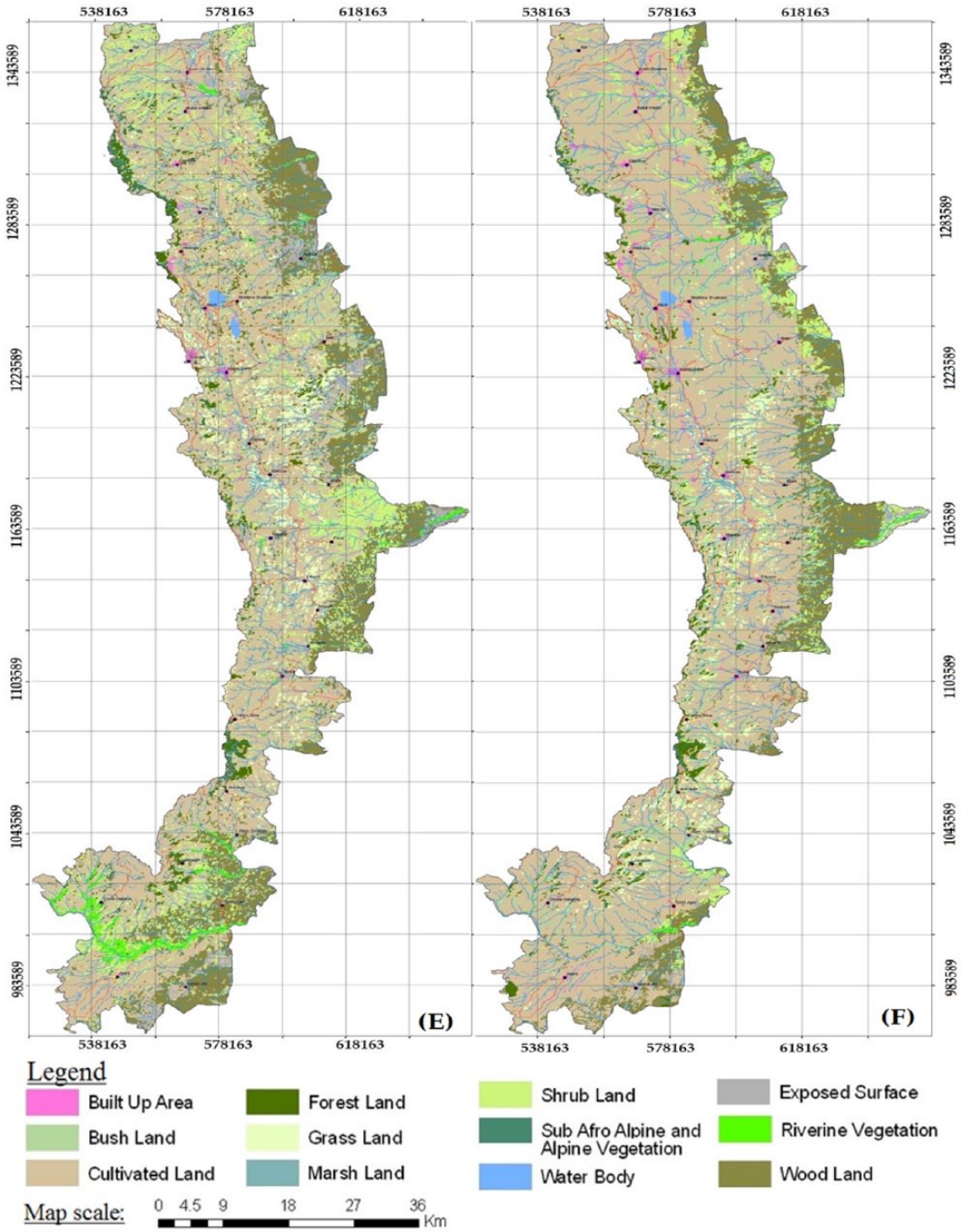

Figure 11. Land cover map: (E) 1995 and (F) 2014.

and 0.1% of the total area for increasing order of slopes indicated in the table. The distribution of the other land cover units can also be statisticized from the tabular data. The relation between terrain slope and land cover units for the year 2014 is detailed in Table 4. The slope map of the area (Figure 12, left) and the land use, soil, and slope overlay map for the country at large (Figure 12, right) were presented to spatially cross-reference the distribution of different land cover units with soil and terrain slope for the study area.

In general, the major proportion of the area for each slope range was covered by cultivated land. From the row total column, rounded to the nearest 10th, it can be seen that following the cultivated land (62.8%), wood (12.4%), bush (8.4%), shrub (6.1%), and grass (4.1%) land units accounted 31% of the total area. The remaining 7 land cover units covered nearly 6.2% of the entire area. The significant change in cultivated land areas across the slope was mainly due to accelerated human impact with population increase and subsequent agricultural land expansion.

Table 4. Percent terrain slope and distribution of land cover units for the 2014 land cover map.

PERCENT SLOPE CLASS AND AREA COVERAGE (HECTARES)								
MAJOR LAND UNIT	0%-2%	2%-5%	5%-8%	8%-15%	15%-30%	30%-60%	>60%	ROW TOTAL %
Built-up	66	4683	719	5662	2812	1206	57	0.81
Bushland	99	956	506	5854	31411	106775	11588	8.37
Cultivated land	9697	139918	40195	218637	336931	403052	30043	62.78
Woodland	473	15332	1701	8167	5778	5045	157	1.95
Exposed surface	175	1019	11	752	3064	22521	15701	2.30
Forest land	1601	6694	192	2849	11508	46323	8316	4.13
Grassland	1302	943	0	36	9	153	14	0.13
Marshland	79	2097	33	728	1549	2372	99	0.37
Riparian vegetation	765	24042	3971	18310	23841	38160	5777	6.12
Shrubland	0	0	0	288	539	3292	3636	0.41
Afro-alpine veg.	4012	81	0	49	46	62	0	0.23
Water body	1456	38439	8006	66470	71533	45865	978	12.40
								100.00
Column total area, hectares	19725	234204	55334	327802	489021	674826	76366	1877278
Column total %	1.1	12.5	2.9	17.5	26.0	35.9	4.1	100.00

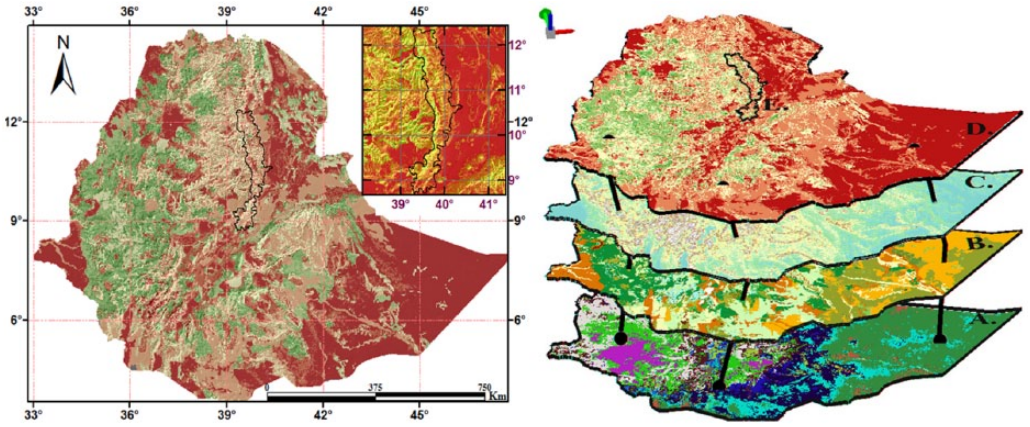

Figure 12. Slope gradient of the study area in the country map (left) and overlay analysis (right): (A) land use, (B) soil, (C) slope, (D) overlay, and (E) study area overlay map.

Implementation of various land management practices and human choices of land use has changed over time due to the impacts of land elevation. In addition, the climate of the area greatly varies with elevation from mountain ridges to valley bottoms influencing the different land use classes. The elevation-land cover area relationship with varying slope ranging from 0% to more than 60% (Table 4, Figure S3) clearly indicated that the elevation distribution of each land use type was different. The ML land cover classification for the year 2014 (Figure S3, Table 4) showed that the distribution of land cover units correlates reasonably well with the variations in terrain slope. There is a general perception that

agricultural areas tend to expand towards soils that are suitable for agriculture.

Conclusions

Human-induced LULC alterations affect the patterns of climate, natural hazard, and socioeconomic dynamics at local and global scales. As a result, mapping LULC changes is essential for a wide range of applications, including landslide, erosion, and land planning activities. In this research, the rate, trend, and magnitude of land cover change for the past 2 decades, 1995 to 2014, were quantified in a 18 772.78-km^2 study area. The area was experiencing a considerable amount of environmental change in the form of deforestation, cultivation, and development activities. For detailed analysis of the spatiotemporal change dynamics, we employed pre-NDVI and object-based supervised classification technique that uses the Bayesian ML classification. Post-classification comparison approach was used to analyse the LULC change between initial and final state images.

The time series analysis of land cover change study proved that there were 12 major land cover units, namely, cultivated, woodland, built-up, bush, exposed surface, forest, grass, marsh, riparian forest, shrub, afro-alpine, and water body. Each of these land use types was influenced by the landform, soil, climate, and human activities. The natural woody vegetation, bush, and shrubland units had been tremendously converted to cultivated land. The study based on 2014 using cloud-free Landsat TM image and field survey revealed that about 63% of the land was in actual cultivation. Of which intensive cultivation covered about 35% of the entire cultivated area and the remaining 65% in the mapping unit comprised scattered and moderately cultivated lands. The expansion of cultivated land was higher (11.14% change) for the past decade, from 2005 to 2014, due to rapid increase in population and resettlement.

In 2014, the largest cultivated land portion of the corridor inventoried in the area indicated that almost all potential agricultural areas in the mid-altitude were under cropping. A substantial portion of the study area (4.13%) was covered by different categories of grassland, whereas afro-alpine and sub-afro-alpine vegetation, forest, woodland, and shrubland units covered 0.41%, 2.3%, 12.4%, and 6.11% of the land area, respectively. Lowland plain areas which had been under dense and open woodlands and wooded grasslands were converted to croplands by resettlers from highlands and intervention of investors producing cash crops. Considering the decadal analysis of LULC change, the spatial extent of agricultural areas has shown an amplified response at the expense of other land use units.

The elevation-land cover area relationship (based on 2014 image analysis) with slope ranging from 0% to more than 60% showed that the elevation distribution of each land use type was different. There was a significant change in cultivated land areas across the slope due to accelerated human impact and subsequent need for arable lands. The result of this study provides a vital monitoring basis for continuous investigations of changes in the natural vegetation and will help decision makers to develop plans to effectively manage their land resources.

ACKNOWLEDGEMENTS

Gebiaw T. Ayele would like to acknowledge Bahir Dar University -Blue Nile Water Institute for financing the research under the project "Remote sensing approaches to access drought severity from multi-temporal GIMMS NDVI, rainfall and PDSI interactions for future drought monitoring".

Author Contributions

GTA and AKT conceived and designed the research and analysed the data and wrote the first draft of the manuscript. GTA, AKT, SSD, MAB, MAJ, and WMT made critical revisions and approved the final version. All the authors contributed to the writing of the manuscript, revisions, and agree with manuscript results and conclusions. All authors reviewed and approved the final manuscript.

REFERENCES

1. Turner BL, Moss RH, Skole DL. *Relating Land Use and Global Land-Cover Change*. Stockholm, Sweden: International Geosphere-Biosphere Programme (Report 24); Barcelona, Spain: Human Dimensions of Global Environmental Change Programme (Report 5).
2. Tilman D, Clarence L. Human-caused environmental change: impacts on plant diversity and evolution. *Proc Nat Acad Sci*. 2001;98:5433–5440.
3. Mustard JF, Defries RS, Fisher T, Moran E. Land-use and land-cover change pathways and impacts. In: Gutman G, Janetos AC, Justice CO, eds. *Land Change Science (Remote Sensing and Digital Image Processing)*. Dordrecht, The Netherlands: Springer; 2012:6.
4. Thilagavathi N, Subramani T, Suresh M. Land use/land cover change detection analysis in Salem Chalk Hills, South India using remote sensing and GIS. *Disaster Adv*. 2015;8:44–52.
5. Hurni H, Solomon A, Amare B, et al. Land degradation and sustainable land management in the highlands of Ethiopia. In: Hurni H, Wiesman UM, eds. *Global Change and Sustainable Development: A Synthesis of Regional Experiences from Research*. Bern, Switzerland: Geographica Bernesia; 2010:187–207.
6. Zewdie W, Elmar C. Remote sensing based multi-temporal land cover classification and change detection in northwestern Ethiopia. *Eur J Remote Sens*. 2015;48:121–139.
7. Ayele GT, Demessie SS, Mengistu KT, Tilahun SA, Melesse AM. Multitemporal land use/land cover change detection for the Batena Watershed, Rift Valley Lakes Basin, Ethiopia. In: Melesse MA, Abtew W, eds. *Landscape Dynamics, Soils and Hydrological Processes in Varied Climates*. New York, NY: Springer International Publishing; 2016:51–72.
8. Swinne E, Veroustaete F. Extending the SPOT-VEGETATION NDV time series (1998-2006) back in time with NOAA-AVHRR data (1985-1998) for Southern Africa. *IEEE Trans Geosci Remote Sens*. 2008;46:558–572.
9. Xu W, Gu S, Zhao X, et al. High positive correlation between soil temperature and NDVI from 1982 to 2006 in alpine meadow of the Three-River Source Region on the Qinghai-Tibetan Plateau. *Int J Appl Earth Obs Geoinf*. 2011;13:528–535.
10. Suleiman YM, Saidu S, Abdulrazaq SA, Hassan AB, Abubakar AN. The dynamics of land use land cover change: using geospatial techniques to promote sustainable urban development in Ilorin Metropolis, Nigeria. *AREES*. 2014;1:8–15.
11. Sexton JO, Urban DL, Donohue MJ, Song C. Long-term land cover dynamics by multi-temporal classification across the Landsat-5 record. *Remote Sens Environ*. 2013;128:246–258.
12. Asres RS, Tilahun SA, Ayele GT, Melesse AM. Analyses of land use/land cover change dynamics in the upland watersheds of Upper Blue Nile Basin. In: Melesse MA, Abtew W, eds. *Landscape Dynamics, Soils and Hydrological Processes in Varied Climates*. New York, NY: Springer International Publishing; 2016:73–91.

13. Prakasam C. Land use and land cover change detection through remote sensing approach: a case study of Kodaikanal taluk, Tamil Nadu. *Int J Geomatics Geosci*. 2010;1:150–158.
14. Reis S. Analyzing land use/land cover changes using remote sensing and GIS in Rize, North-East Turkey. *Sensors*. 2008;8:6188–6202.
15. Lu D, Mausel P, Batistella M, Moran E. Land-cover binary change detection methods for use in the moist tropical region of the Amazon: a comparative study. *Int J Remote Sens*. 2005;26:101–114.
16. Bastin L. Comparison of fuzzy c-means classification, linear mixture modelling and MLC probabilities as tools for unmixing coarse pixels. *Int J Remote Sens*. 1997;18:3629–3648.
17. Lillesand T, Kiefer RW, Chipman J. *Remote Sensing and Image Interpretation*. Hoboken, NJ: John Wiley & Sons; 2014.
18. Muzein BS. *Remote Sensing & GIS for Land Cover/ Land Use Change Detection and Analysis in the Semi-Natural Ecosystems and Agriculture Landscapes of the Central Ethiopian Rift Valley*. Dresden, Germany: Technische Universität Dresden; 2006:66–70.
19. Kolios S, Stylios CD. Identification of land cover/land use changes in the greater area of the Preveza peninsula in Greece using Landsat satellite data. *Appl Geogr*. 2013;40:150–160.
20. Dezso Z, Bartholy J, Pongracz R, Barcza Z. Analysis of land-use/land-cover change in the Carpathian region based on remote sensing techniques. *Phys Chem Earth*. 2005;30:109–115.
21. Wilkie DS, Finn JT. *Remote Sensing Imagery for Natural Resources Monitoring*. New York, NY: Columbia University Press; 1996.
22. Abd El-Kawy OR, Rød JK, Ismail HA, Suliman AS. Land use and land cover change detection in the western Nile delta of Egypt using remote sensing data. *Appl Geogr*. 2011;31:483–494.
23. Yeshaneh E, Wagner W, Exner-Kittridge M, Legesse D, Blöschl G. Identifying land use/cover dynamics in the Koga Catchment, Ethiopia, from multi-scale data, and implications for environmental change. *ISPRS Int J Geo Inf*. 2013;2:302–323.
24. Rawat JS, Kumar M. Monitoring land use/cover change using remote sensing and GIS techniques: a case study of Hawalbagh block, district Almora, Uttarakhand, India. *EJRS*. 2015;18:77–84.
25. Mas JF. Monitoring land-cover changes: a comparison of change detection techniques. *Int J Remote Sens*. 1999;20:139–152.
26. Jemberie MA, Awass AA, Melesse AM, Ayele GT, Demissie SS. Seasonal rainfall-runoff variability analysis, Lake Tana Sub-Basin, Upper Blue Nile Basin, Ethiopia. In: Melesse MA, Abtew W, eds. *Landscape Dynamics, Soils and Hydrological Processes in Varied Climates*. New York, NY: Springer International Publishing; 2016:341–363.
27. Ayele GT, Teshale EZ, Yu B, Rutherfurd ID, Jeong J. Streamflow and sediment yield prediction for watershed prioritization in the Upper Blue Nile River Basin, Ethiopia. *Water*. 2017;9:782.
28. Haile T, Yarotskaya L. *Onset and Cessation of Rains in Ethiopia*. Addis Ababa, Ethiopia: NMSA; 1987.
29. MoA. *Agroecological Zonations of Ethiopia*. Addis Ababa, Ethiopia: Ministry of Agriculture; 2000.
30. NMSA. *Climatic and Agroclimatic Resources of Ethiopia*. Addis Ababa, Ethiopia: National Meteorology Service Agency;1996.
31. Hurni H. *Agroecological Belts of Ethiopia: Explanatory Notes on Three Maps at a Scale of 1:1,000,000, Soil Conservation Research Program of Ethiopia*. Addis Ababa, Ethiopia: Ministry of Agriculture; 1998.
32. Walker S, Getahun YG, Tesfaye K, Mamo G, Yeshanew A, Bekele E. The use of agroclimatic zones as a basis for tailored seasonal rainfall forecasts for the cropping systems in the central rift valley of Ethiopia. Paper presented at: Insights and Tools for Adaptation: Learning from Climate Variability; November18-20, 2003; Washington, DC:1–7.
33. NASA LP DAAC. ASTER DEM Product (Data Set). https://doi.org/10.5067/ASTER/AST14DEM.003. Accessed December 21, 2015.
34. Wu Q_, Hong-qing L, Ru-song W, et al. Monitoring and predicting land use change in Beijing using remote sensing and GIS. *Landsc Urban Plan*. 2006;78:322–333.
35. Roy D, Junchang J, Kristi K, et al. Web-enabled Landsat Data (WELD): landsat ETM+ composited mosaics of the conterminous United States. *Remote Sens Environ*. 2010;114:35–49.
36. Ju J, David P, Eric V, Jeffrey M, Valeriy K. Continental-scale validation of MODIS-based and LEDAPS Landsat ETM+ atmospheric correction methods. *Remote Sens Environ*. 2012;122:175–184.
37. Dodgson NA. *Image Resampling (No. UCAM-CL-TR-261)*. Cambridge, UK: University of Cambridge (Computer Laboratory); 1992.
38. Crippen RE. A simple spatial filtering routine for the cosmetic removal of scan-line noise from landsat TM P-tape imagery. *Photogramm Eng Rem S*. 1989;55:327–331.
39. Richards J. *Remote Sensing Digital Image Analysis: An Introduction*. Berlin, Germany: Springer-Verlag; 1999.
40. Bakker WH, Grabmaier KA, Hunmeman GC, et al. *Principles of Remote Sensing, an Introductory Textbook*. Enschede, the Netherlands: The International Institute for Geo-Informational Science and Earth Observation (ITC); 2004.
41. Serra P, Pons X, Sauri D. Post-classification change detection with data from different sensors: some accuracy considerations. *Int J Remote Sens*. 2003;24:3311–3340.
42. Parker JA, Kenyon RV, Troxel DE. Comparison of interpolating methods for image resampling. *IEEE Trans Med Imaging*. 1983;2:31–39.
43. Seka AM, Awass AA, Melesse AM, Ayele GT, Demissie SS. Evaluation of the effects of water harvesting on downstream water availability using SWAT. In: Melesse MA, Abtew W, eds. *Landscape Dynamics, Soils and Hydrological Processes in Varied Climates*. New York, NY: Springer International Publishing; 2016:763–787.
44. Lu D, Li G, Kuang W, Moran E. Methods to extract impervious surface areas from satellite images. *Int J Digit Earth*. 2014;7:93–112.
45. Blaschke T. Object based image analysis for remote sensing. *ISPRS J Photogramm Remote Sens*. 2010;65:2–16.
46. Melesse AM, Jordan JD. A comparison of fuzzy vs. augmented-ISODATA classification algorithm for cloud and cloud-shadow discrimination in Landsat images. *Photogram Eng Remote Sens*. 2002;68:905–911.
47. Sánchez-Reyes UJ, Niño-Maldonado S, Barrientos-Lozano L, Treviño-Carreón J. Assessment of land use-cover changes and successional stages of vegetation in the natural protected area Altas Cumbres, Northeastern Mexico, using Landsat satellite imagery. *Remote Sensing*. 2017;9:1–33.
48. Asmala A. Analysis of maximum likelihood classification on multispectral data. *Appl Mathematic Sci*. 2012;6:6425–6436.
49. Alzer H, Berg C. Some classes of completely monotonic functions, II. *Ramanujan J*. 2006;11:225–248.
50. Anderson JR. *A Land Use and Land Cover Classification System for Use With Remote Sensor Data*. Washington, DC: US Government Printing Office; 1976.
51. Verbyla D. Potential prediction bias in regression and discriminant analysis. *Can J For Res*. 1986;16:1255–1257.
52. Congalton R. A review of assessing the accuracy of classification of remotely sensed data. *Remote Sens Environ*. 1996;37:35–46.
53. Ozesmi SL, Bauer ME. Satellite remote sensing of wetlands. *Wetl Ecol Manag*. 2002;10:381–402.
54. Ayele GT, Demissie SS, Tilahun SA, et al. Assessing drought severity from multi-temporal GIMMSNDVI and rainfall interactions. In: *36th Hydrology and Water Resources Symposium: The art and science of water*. Barton, ACT: Engineers Australia, Tasmania, Australia, 7–10 December 2015; 306–314.
55. Garrigues S, Allard D, Baret F. Using first-and second-order variograms for characterizing landscape spatial structures from remote sensing imagery. *IEEE Trans Geosci Remote Sens*. 2007;45:1823–1834.
56. Myneni RB, Hall FG, Sellers PJ, Marshak AL. Interpretation of spectral vegetation indexes. *IEEE Trans Geosci Remote Sens*. 1995;33:481–486.
57. Hassan Z, Shabbir R, Ahmad SS, et al. Dynamics of land use and land cover change (LULCC) using geospatial techniques: a case study of Islamabad Pakistan. *Springer Plus*. 2016;5:812.